

## Decoding Sources of Energy Variability in a Laser-Plasma Accelerator

Andreas R. Maier<sup>1,2,\*</sup> Niels M. Delbos,<sup>1</sup> Timo Eichner,<sup>1</sup> Lars Hübner,<sup>1,2</sup> Sören Jalas,<sup>1</sup> Laurids Jeppe,<sup>1</sup>  
 Spencer W. Jolly<sup>1,3</sup> Manuel Kirchen<sup>1</sup> Vincent Leroux<sup>2,1,3</sup> Philipp Messner,<sup>4,1</sup>  
 Matthias Schnepf,<sup>1</sup> Maximilian Trunk,<sup>1</sup>  
 Paul A. Walker,<sup>2,1</sup> Christian Werle,<sup>1</sup> and Paul Winkler<sup>2,1</sup>

<sup>1</sup>*Center for Free-Electron Laser Science and Department of Physics Universität Hamburg,  
 Luruper Chaussee 149, 22761 Hamburg, Germany*

<sup>2</sup>*Deutsches Elektronen Synchrotron (DESY), Notkestraße 85, 22607 Hamburg, Germany*

<sup>3</sup>*Institute of Physics of the ASCR, ELI-Beamlines Project, Na Slovance 2, 18221 Prague, Czech Republic*

<sup>4</sup>*International Max Planck Research School for Ultrafast Imaging & Structural Dynamics,  
 Luruper Chaussee 149, 22761 Hamburg, Germany*



(Received 7 April 2020; accepted 23 July 2020; published 18 August 2020)

Laser-plasma acceleration promises compact sources of high-brightness relativistic electron beams. However, the limited stability often associated with laser-plasma acceleration has previously prevented a detailed mapping of the drive laser and electron performance and represents a major obstacle towards advancing laser-plasma acceleration for applications. Here, we correlate drive laser and electron-beam parameters with high statistics to identify and quantify sources of electron energy drift and jitter. Based on our findings, we provide a parametrization to predict the electron energy drift with subpercent accuracy for many hours from measured laser parameters, which opens a path for performance improvements by active stabilization. Our results are enabled by the first stable 24-h operation of a laser-plasma accelerator and the statistics from 100 000 consecutive electron beams, which, by itself, marks an important milestone.

DOI: [10.1103/PhysRevX.10.031039](https://doi.org/10.1103/PhysRevX.10.031039)

Subject Areas: Photonics, Plasma Physics

### I. INTRODUCTION

Highly relativistic, high-brightness electron beams are an essential tool for fundamental and life-science research. Laser-plasma acceleration (LPA) [1,2] promises to increase the availability of this important resource at significantly reduced size and cost compared to modern radio-frequency (RF) based accelerators.

In a LPA, the interaction of an intense laser pulse with a plasma creates a trailing cavity, a plasma wave, which traps and accelerates electrons from the plasma background [2]. This cavity supports electric fields several orders of magnitude higher than in a modern RF accelerator, which reduces the distance required to generate giga-electron-volt-level electron beams from kilometers to centimeters [3–6].

Milestone experiments have verified key principles of laser-plasma acceleration and the possibility to generate high-brightness beams, featuring electron bunches of low emittance [7,8], few-femtosecond (fs) length, and

kiloampere peak current [9–11]. Advanced concepts have demonstrated novel injection techniques [12–14] and the generation of plasma-driven x-ray pulses [15–18]. These results show that laser-plasma accelerators are, in principle, capable of generating electron beams with competitive beam quality. However, it is still a major challenge to produce those beams reliably and reproducibly.

Unlike RF-based machines, a laser-plasma accelerator generates a new accelerating cavity with every shot. Thus, small fluctuations in the experimental conditions, in particular, those associated with the drive laser properties, can cause significant shot-to-shot variation (jitter) in the electron-beam performance. In addition, longer-term evolution in the complex drive laser often prevents consistent operation of the setup. As a consequence, the number of events in a typical experiment is low, and high-quality electron beams represent the exception rather than the rule for many laser-plasma acceleration results.

Operating with limited statistics is a major obstacle to the desired goal of advancing laser-plasma acceleration for applications. It hinders mapping correlations between parameters and performance, results in an incomplete picture of the precise mechanics underlying laser-plasma acceleration, and prevents a detailed understanding of which key parameters must be controlled to reproducibly achieve high-quality electron beams. Adopting a high-statistics experimental approach is thus an important next step.

\*andreas.maier@desy.de

*Published by the American Physical Society under the terms of the Creative Commons Attribution 4.0 International license. Further distribution of this work must maintain attribution to the author(s) and the published article's title, journal citation, and DOI.*

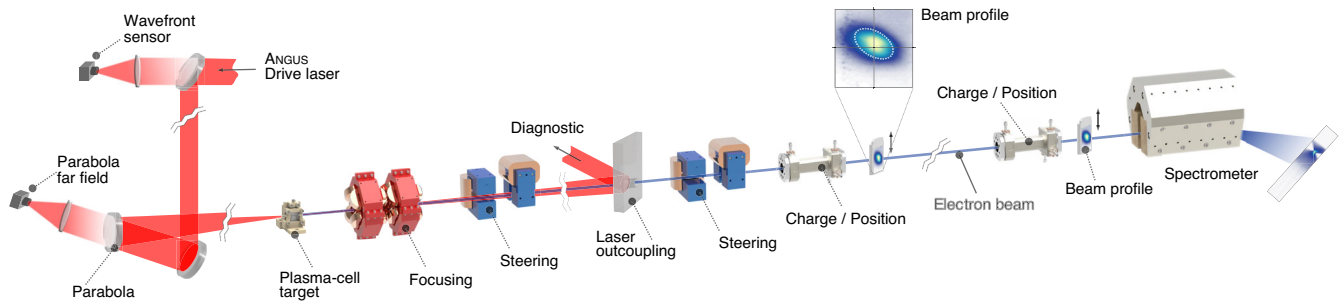


FIG. 1. The drive laser (red) is focused into a plasma-cell target, where it ionizes a nitrogen-doped hydrogen gas to form a plasma and then traps and accelerates electrons to an energy of 368 MeV. After the target, the laser is extracted from the beam axis for diagnostics. The electron beam (blue) is captured using a pair of electromagnetic quadrupoles and focused into a permanent magnet dipole spectrometer. The electron beam is adjusted to the accelerator design axis using steering dipoles. Retractable scintillating screens and cavity-type beam position monitors provide electron-beam profile, charge, and position information. For clarity, only a few of the installed laser diagnostics are shown. The whole setup is integrated into a controls system to enable live monitoring, tuning, and processing of the acquired data.

Here, we correlate laser and electron parameters using the unprecedented statistics from more than 100 000 consecutive electron beams generated at a 1-Hz repetition rate. Our study is only enabled by the first continuous 24-h operation of a laser-plasma-based accelerator, which performs with sufficient stability to effectively limit parameter variations while providing comprehensive diagnostics to access a mapping of drive laser and electron parameters. Based on these correlations, we accurately model the electron energy using measured laser data and explain and quantify main sources of the residual electron energy drift and jitter. Our approach opens the path for feedback loops and active performance control, which is a crucial step required for laser-plasma acceleration to become a driver for applications [19–22].

## II. EXPERIMENTAL SETUP

The LUX accelerator [23], shown in Fig. 1, was developed explicitly for the purpose of isolating the sources of variability in laser-plasma acceleration. The primary driver underlying the design is the combination of the state of the art in laser-plasma and modern accelerator technology. By achieving reproducible operation, we limit the system’s degrees of freedom, which is crucial to extract correlations from the extensive data set.

The plasma accelerator is driven by the ANGUS laser, a Ti:Sapphire-based chirped-pulse amplification system, which, for this campaign, provided 2 J ( $\pm 1.8\%$  rms) pulse energy on target (3.5 J before the compressor) at 42 fs FWHM pulse length to deliver 48 TW peak power at a 1-Hz repetition rate. The laser was focused (Strehl ratio 0.9) to a spot size of 25  $\mu\text{m}$  FWHM with a 2-m focal length off-axis parabolic mirror (parabola) into a plasma-cell target and extracted for postinteraction analysis using a glass wedge with an on-axis hole.

As a key to stable laser operation, we systematically diagnosed the laser pulse as it evolved from its origin in the femtosecond oscillator through the following amplification

and pulse-shaping stages. At each interface between subsequent stages, we live monitored a defined set of laser pulse properties, such as spectrum, energy, and beam profile, and actively stabilized the laser path.

The plasma target was machined from a sapphire crystal. A square (500- $\mu\text{m}$  side length) channel was continuously filled with hydrogen from two independently mass-flow-controlled inlets to support a 4-mm plasma density plateau of  $2.7 \times 10^{18} \text{ cm}^{-3}$  electron density. The pressure, measured directly at the inlets, was 55.5 mbar and 56.5 mbar, respectively. The first inlet was doped with nitrogen (up to 3% concentration) to inject electrons from ionization injection [24–26] and accelerate them to an energy of 368 MeV. A differential pumping stage removed the gas load from the target chamber. The target supported in excess of 200 000 shots before replacement.

To set up the electron beam for the data run, we had access to different parameters. We scanned the laser focus position and set it at a position within the plasma density up-ramp where the resulting electron energy jitter was low (compare also the discussion of our experimental results below). In addition, we varied the laser energy using an attenuator located just before the compressor. In general, for a fixed spot size, a higher laser energy increases the transverse injection volume, leading to higher charge, larger divergence, and larger emittance. Operation at lower laser energies supported less beam charge but was preferred to increase the transverse quality of the injected beam. We balanced the reduction in charge from lower laser energies by slightly increasing the dopant concentration. Furthermore, we could slightly adjust the resulting energy spread by tuning the beam loading via the beam charge, i.e., with laser energy and dopant concentration.

Note, however, that the goal of this campaign was not to optimize a particular electron-beam property like energy, charge, energy spread, or emittance, but to demonstrate continuous delivery of reproducible electron beams. The optimization of the electron bunch properties by dedicated

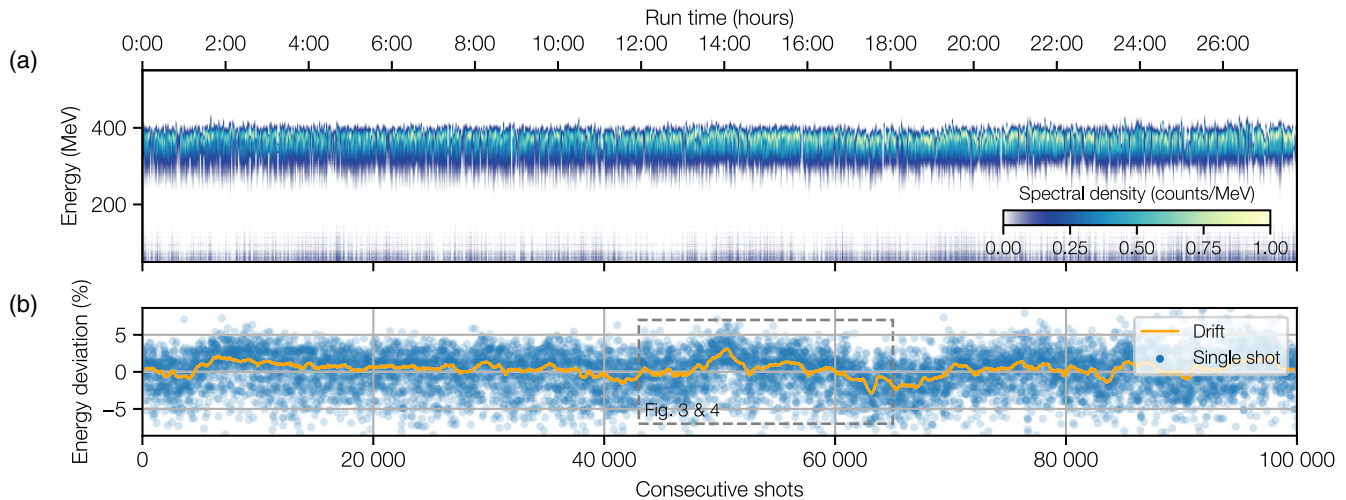


FIG. 2. Panel (a) shows the energy spectra of 100 000 consecutive laser-plasma generated electron beams. Here, each line represents one single shot. The camera images of the electron spectrometer screen are background corrected, projected onto the dispersive axis, and calibrated to a linear energy scale. The peak energy of each spectrum (dots) is shown in panel (b), together with the energy drift (solid line) calculated as the rolling average over a 6-min window, i.e., 360 shots. The percent-level energy drift can be attributed to a drift in drive laser parameters (compare Figs. 3 and 4).

tuning of the machine will be the subject of separate publications.

Electron beams, generated from the laser-plasma interaction, were captured by a pair of electromagnetic quadrupoles and focused into the spectrometer—a permanent magnet dipole, which disperses the electron beam onto a scintillating screen. At 368-MeV electron energy, the spectrometer resolution was 1%.

Focusing the electron beams into the spectrometer is essential to achieve the energy resolution required for our analysis. The electron-beam optic defines a spectral transmission function [27]. The transmission dropped to 75% for energies below 300 MeV and was more than 90% for energies around  $\pm 10\%$  of the focused electron energy. We carefully ensured that the transmission of the electron beam line did not affect our analysis. However, it effectively suppressed the low-energy tail of the spectrum, which is typical for many ionization-injection schemes.

To noninvasively measure the transverse position of the electron beam, we use cavity-type beam-position monitors (BPM), which derive the beam position from the electric field induced by the electron beam as it passes the cavity. The BPMs are absolutely calibrated to provide the charge of the passing electron bunch.

### III. RESULTS

We operated the LUX accelerator continuously to generate 100 000 consecutive electron beams at a 1-Hz repetition rate, shown in Fig. 2. The electron beams had, on average, a peak energy of 368 MeV ( $\pm 2.4\%$  rms), a charge of 25 pC ( $\pm 11\%$  rms), and a FWHM energy spread of 54 MeV ( $\pm 15$  MeV rms). Statistics were calculated over the full set of shots. The absolute number of consecutive

shots outperforms previously reported laser-plasma results by orders of magnitude and enables studies with unprecedented statistics.

The electrons had a divergence of 1.8 mrad and a pointing jitter of 0.8 mrad rms and 0.7 mrad rms in both transverse planes.

Figure 2(b) shows the peak energy of individual shots (dots) and the rolling average (solid line) over a 6-min window, i.e., 360 shots, which we define as the energy drift. On average, the electron energy remained constant over the run and featured only slow drifts on a few-percent scale. This steady performance indicates the robustness of the machine, despite the slow change of the environmental conditions due to the passage from day into night and back, which is a common cause of a degrading performance.

Since energy stability is a crucial figure of merit for accelerator performance, we focused on the electron energy as the primary output parameter. Laser-plasma acceleration is governed by complex, yet deterministic, dynamics. It can be expected that variations in only a few laser properties are responsible for the bulk of the variation in electron energy.

In the following, we present an analysis of both the long-term stability (energy drift) and the shot-to-shot stability (energy jitter). We used a 2-h window of approximately 7000 shots from the 24-h run presented in Fig. 2 as a training set to determine correlations between electron energy and a few selected laser parameters. The primary factors determining the electron energy seemed to be (a) the laser energy, (b) the longitudinal focus position, and (c) the laser direction at the focusing parabola. The correlations, presented in Fig. 3, can be understood as follows.

First, a higher-energy laser drives a stronger wakefield, i.e., accelerating gradient, and thus supports higher electron

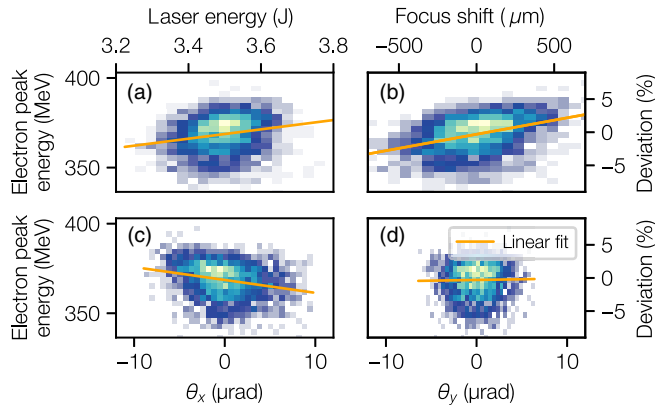


FIG. 3. (a) Electron peak energy correlated with the laser energy  $E$ , measured from a mirror leakage after the main amplifier. (b) Longitudinal laser focus position, measured with a wavefront sensor after the compressor. (c,d) Laser angle of incidence  $\theta$  (pointing), derived from the far field behind the parabola. The correlations are based on a 2-h data subset, as indicated in Fig. 4. The orange line is a linear fit to the correlation. The positions of the wavefront and far-field measurement are shown in Fig. 1.

energies [Fig. 3(a)]. In our experiment, the laser intensity increased to  $a_0 \approx 3$  due to self-focusing. For the nonlinear blowout regime, Lu *et al.* [28] predict a scaling of the electron energy  $\mathcal{E}$ , with laser intensity  $\mathcal{E} \propto a_0^{1/2}$ . Thus,  $\mathcal{E} \propto P^{1/4} \propto E^{1/4} \times \tau^{-1/4}$ , with  $P$  the laser power,  $E$  the laser energy, and  $\tau$  the laser pulse length. It is straightforward to expand this relation to first order and linearly approximate the electron energy as a function of laser energy,  $\Delta\mathcal{E}(E)/\mathcal{E}_0 \approx 1/4 \times \Delta E/E_0$ , with  $\Delta E = E - E_0$ ,  $\Delta\mathcal{E} = \mathcal{E} - \mathcal{E}_0$ , and  $\mathcal{E}_0$  and  $E_0$  the mean electron peak energy and mean laser pulse energy, respectively. The linear fit to the correlation shown in Fig. 3(a), but expressed in scaled variables  $\Delta\mathcal{E}/\mathcal{E}_0$  and  $\Delta E/E_0$ , results in  $\Delta\mathcal{E}(E)/\mathcal{E}_0 \approx 0.24 \times \Delta E/E_0$ . The experimentally derived scaling matches well with the predicted scaling [28]. It confirms that we operated in a regime where the energy gain of the electron beam is determined by the length of the acceleration distance not by dephasing.

Second, higher electron energies are generated for a positive focus shift, Fig. 3(b). We define a positive focus shift in the direction towards the plasma density plateau. The mechanism behind this correlation is a combination of laser self-focusing, the resulting evolution of the laser intensity along the target, and the injection dynamics.

The maximum  $a_0$  increases as the focus is shifted in the positive direction along the plasma density up-ramp. In addition, simulations show that the injection dynamic depends on the focus position: Shifting the focus in the positive direction, the current profile steepens at the head of the injected bunch, which changes the beam-loading field and additionally increases the average accelerating field at the head of the beam. Thereby, the energy in the peak increases.

The slope of a correlation such as presented in Fig. 3(b) corresponds to the electron energy jitter that is caused by the wavefront-induced focus jitter. In our experiment, it was about  $200 \mu\text{m}$  rms—a result of air fluctuations and nonlinearities within the laser, which influence the shot-to-shot jitter in the wavefront. As we have confirmed with a dedicated scan, the electron peak energy increases slightly nonlinearly as we shift the focus along the plasma density up-ramp. The wavefront-induced focus jitter thus causes a larger electron energy jitter for focus positions closer to the plasma density plateau. During the initial tuning of the experiment, we set the focus position such that the electron energy jitter was small. Simulations show that this is consistent with a focus position in the second half of the density up-ramp, which also agrees with an independent measurement of the focus position.

Third, we observed a correlation of the electron peak energy with the laser direction (pointing) measured at the focusing parabola. The electron energy depended on the laser pointing in the  $x$  direction but seemed to be unaffected by the laser pointing in the  $y$  direction [Figs. 3(c) and 3(d)]. Intuitively, a change in laser pointing should not directly affect the electron-beam energy.

The laser pointing measured at the parabola is connected to the laser pointing into the pulse compressor. The fact that we observed a correlation of electron energy with the laser direction in  $x$  (the dispersive plane of the compressor) suggests that the laser direction couples via the pulse length to the electron energy. This mechanism would be consistent with our observation that the pointing jitter in the non-dispersive plane ( $y$  direction) did not correlate with the electron energy. The changes in pulse length induced by the measured pointing jitter of  $3 \mu\text{rad}$  are, however, too small to explain the resulting energy jitter.

Other mechanisms that might also explain our observations include additional variations of the wavefront; a transversely inhomogeneous target density; or pointing-induced changes of spatiotemporal couplings in the drive pulse, which are likely present due to heat-induced deformations of the compressor gratings [29–31].

Note that the  $3\text{-}\mu\text{rad}$  pointing jitter measured at the parabola is small, but it is typical for a TW-class laser system. It resulted in a subpercent electron energy variation. Although a clarification of the exact mechanism behind the correlation will require further study, it highlights the benefits of using high statistics, which enabled us to identify and quantify an effect that would otherwise likely have been hidden in the data. As a preventive measure, we actively stabilized slow changes of the laser pointing before the compressor entrance. The correlations in panels (c) and (d) are the result of additional residual pointing variations or ones that are not yet fully corrected.

To test the quality of our data, we used the measured correlations, Fig. 3, to generate a first-order parametrization

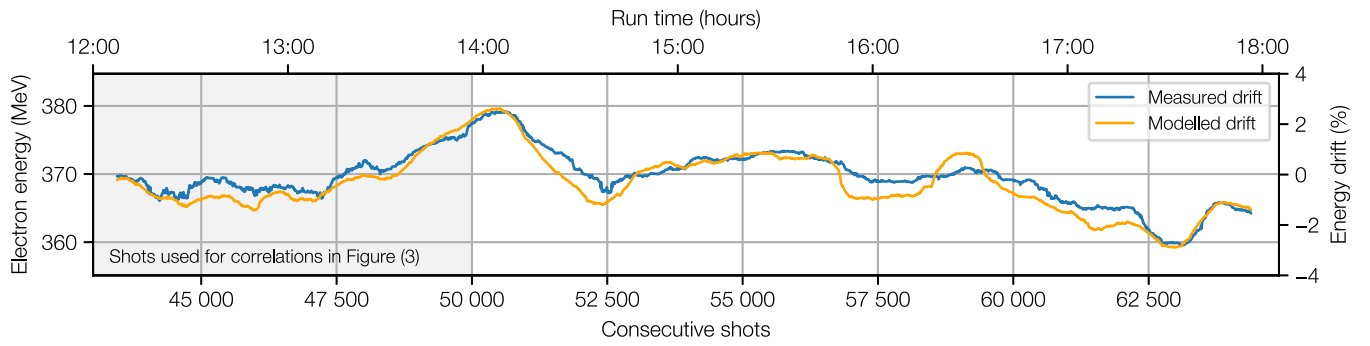


FIG. 4. To model the measured electron energy drift (blue), we used Eq. (1), the correlations presented in Fig. 3, and the drift of the measured laser energy, laser focus shift, and laser direction. As before, we calculated the drift as the 6-min rolling average (360 shots) of the single-event data. Only four noninvasively measured laser parameters are sufficient to predict (orange) the evolution of the electron energy with subpercent accuracy. The modeled electron energy is accurate for a 6-h (22 000 shots) time span, which significantly exceeds the 2-h time window (7000 shots) we used to correlate the laser and electron data.

of the electron energy. In general, the electron energy is an unknown function  $\mathcal{E}$  of laser parameters. Assuming that the electron energy is, to first order, already well described by the laser energy, the focus shift, and the laser direction at the parabola, the change in the electron energy,  $\Delta\mathcal{E}$ , can be expanded in a Taylor series,

$$\Delta\mathcal{E}(E, Z, \theta) \approx \frac{\partial\mathcal{E}}{\partial E}\Delta E + \frac{\partial\mathcal{E}}{\partial Z}\Delta Z + \frac{\partial\mathcal{E}}{\partial\theta_x}\Delta\theta_x + \frac{\partial\mathcal{E}}{\partial\theta_y}\Delta\theta_y, \quad (1)$$

where  $E$  is the laser energy,  $Z$  is the focus shift, and  $\theta_x$  and  $\theta_y$  describe the laser's angle of incidence at the parabola. To obtain the partial derivatives  $\partial_E\mathcal{E}$ ,  $\partial_Z\mathcal{E}$ , and  $\partial_\theta\mathcal{E}$ , we applied a linear fit to the correlations in Fig. 3 (solid lines). The measured laser data for  $\Delta E$ ,  $\Delta Z$ , and  $\Delta\theta$  could then be used to model the electron energy from Eq. (1).

Figure 4 compares the measured energy drift (blue) with the drift modeled from the four noninvasively measured laser parameters (orange). Note that we used only a 2-h window as a training set for our correlations but could extrapolate the model for as many as 6 h, predicting the electron energy drift with subpercent precision. This level of accuracy indicates that we identified the main laser properties responsible for the drift and that the drift could, in principle, be eliminated by stabilizing those laser properties in a feedback loop.

After 6 h, the accuracy of the model was reduced. Subtle drifts of laser parameters throughout the amplification chain and thermal effects, which included a slow heating of the compressor gratings [30,31] and beam transport optics, slightly changed the correlation terms shown in Fig. 3. By updating the correlations, the accuracy of the model can be recovered. Thereby, the model is extended to cover the full 100 000 shots of the run, as shown in Fig. 5.

In addition to reducing the energy drift, it is essential for many applications to minimize the shot-to-shot energy

variation (jitter), and thus, it is important to understand the origins of these variations. The analysis presented above was based on the rolling average of measured laser parameters and successfully predicted the electron energy drift over a 6-h time window. We then used the single-shot laser data and Eq. (1) to calculate the individual electron energies for all 22 000 shots of this time interval.

The standard deviation of this set, 1.9% rms, can be interpreted as the electron energy jitter over the 6-h time window, predicted by Eq. (1).

Individually, the laser energy, focus position, and laser direction caused 0.7%, 1.0%, and 0.8% of electron energy jitter, respectively. For this estimation, we assumed that the measured variations in laser parameters were large compared to the repeatability of our diagnostics. However, as the contributions of individual laser parameters to the electron energy stability approach the subpercent level, the resolution of current laser diagnostics will need to be carefully considered for future, more-detailed studies. The quadratic sum of the individual jitters was slightly smaller than 1.9%, which indicates that the laser parameters we used for our model were not completely independent.

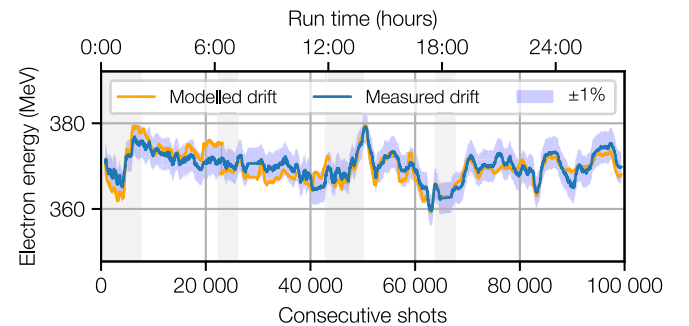


FIG. 5. Gray shaded areas mark the events used to derive the correlations  $\partial_E\mathcal{E}$ ,  $\partial_Z\mathcal{E}$ , and  $\partial_\theta\mathcal{E}$ . By regularly updating the correlations, the parametrization of the electron energy drift can be extended to the full data set.

The difference between measured (2.4%) and predicted jitter (1.9%) further implies that the electron energy depends on additional laser parameters.

The laser pulse length  $\tau$ , for example, is such an important parameter, and is expected to affect the electron energy. Unfortunately, it could not be measured online for every shot and was thus not available for the above analysis. We can, however, estimate the effect of a laser pulse length variation onto the electron energy based on our findings.

After the run, we independently characterized the laser pulse length jitter  $\sigma(\tau)$  to be of order 3% rms. Since the electron energy scales with the laser pulse energy and length as  $\mathcal{E} \propto E^{1/4} \times \tau^{-1/4}$ , we can, to first order, assume that the laser pulse length and laser energy cause a similar relative change in electron energy. Based on Eq. (1), we can then approximate an additional energy jitter of about 0.8% for a pulse length jitter of order 3% rms.

#### IV. CONCLUSION

In our experiment, we used the unprecedented statistics from 100 000 consecutive electron beams to analyze the mapping of laser parameters and electron-beam performance. Stable accelerator operation was a key enabler for this study, as it effectively limited parameter variations. In combination with a comprehensive set of diagnostics, we could then isolate correlations to explain and quantify the most important parameters affecting the electron-beam energy of our target.

Based on the correlations of laser and electron parameters, we could model the electron energy drift with subpercent precision using measured laser data. Such a parametrization of the electron-beam energy is a powerful tool, which enables the future implementation of feedback loops and fine-tuning of the accelerator to generate reproducible electron beams that reach the demanding level of performance required by applications.

Our results show the benefits of operating a laser-plasma experiment with high statistics. It enables a mapping of laser and electron parameters directly from the experiment, a detailed exploration of the nuanced dynamics of laser-plasma acceleration, and a parametrization of the electron-beam properties. Our approach is generally valid and independent of the specific details of the laser-plasma accelerator setup. It could be transferred to and thus benefit other, more complex injection schemes, which are often associated with high-quality beams but are also more sensitive to subtle variations in the drive laser. Adopting continuous high-statistics operation could help to decode the sources of variability in those schemes and thereby significantly improve the reproducibility of high-quality beams.

#### ACKNOWLEDGMENTS

We appreciate support from the workshops and technical groups of Hamburg University and DESY. We thank

N. H. Matlis (DESY) and W. P. Leemans (DESY) for discussions. This work was supported by BMBF Grants No. 05K16GU2, No. 05K19GUA, and No. 05K19GUD; the DESY Strategy Fund; computing time granted on the supercomputer JUWELS (project CHHH20) at Jülich Supercomputing Centre (JSC); and the Horizon2020 Project No. 653782. S. W. J. and V. L. acknowledge support from the European Regional Development Fund (ERDF) (CZ.02.1.01/0.0/0.0/15\_008/0000162).

- 
- [1] T. Tajima and J. M. Dawson, *Laser Electron Accelerator*, *Phys. Rev. Lett.* **43**, 267 (1979).
  - [2] E. Esarey, C. B. Schroeder, and W. P. Leemans, *Physics of Laser-Driven Plasma-Based Electron Accelerators*, *Rev. Mod. Phys.* **81**, 1229 (2009).
  - [3] W. P. Leemans, B. Nagler, A. J. Gonsalves, C. Tóth, K. Nakamura, C. G. R. Geddes, E. Esarey, C. B. Schroeder, and S. M. Hooker, *GeV Electron Beams from a Centimetre-Scale Accelerator*, *Nat. Phys.* **2**, 696 (2006).
  - [4] X. Wang *et al.*, *Quasi-Monoenergetic Laser-Plasma Acceleration of Electrons to 2 GeV*, *Nat. Commun.* **4**, 1988 (2013).
  - [5] W. P. Leemans, A. J. Gonsalves, H.-S. Mao, K. Nakamura, C. Benedetti, C. B. Schroeder, C. Tóth, J. Daniels, D. E. Mittelberger, S. S. Bulanov, J.-L. Vay, C. G. R. Geddes, and E. Esarey, *Multi-GeV Electron Beams from Capillary-Discharge-Guided Subpetawatt Laser Pulses in the Self-Trapping Regime*, *Phys. Rev. Lett.* **113**, 245002 (2014).
  - [6] A. J. Gonsalves *et al.*, *Petawatt Laser Guiding and Electron Beam Acceleration to 8 GeV in a Laser-Heated Capillary Discharge Waveguide*, *Phys. Rev. Lett.* **122**, 084801 (2019).
  - [7] R. Weingartner, S. Raith, A. Popp, S. Chou, J. Wenz, K. Khrennikov, M. Heigoldt, A. R. Maier, N. Kajumba, M. Fuchs, B. Zeitler, F. Krausz, S. Karsch, and F. Grüner, *Ultralow Emittance Electron Beams from a Laser-Wakefield Accelerator*, *Phys. Rev. ST Accel. Beams* **15**, 111302 (2012).
  - [8] G. R. Plateau, C. G. R. Geddes, D. B. Thorn, M. Chen, C. Benedetti, E. Esarey, A. J. Gonsalves, N. H. Matlis, K. Nakamura, C. B. Schroeder, S. Shiraishi, T. Sokollik, J. van Tilborg, C. Tóth, S. Trotsenko, T. S. Kim, M. Battaglia, T. Stöhlker, and W. P. Leemans, *Low-Emittance Electron Bunches from a Laser-Plasma Accelerator Measured Using Single-Shot X-Ray Spectroscopy*, *Phys. Rev. Lett.* **109**, 064802 (2012).
  - [9] O. Lundh, J. Lim, C. Rechatin, L. Ammoura, A. Ben-Ismaïl, X. Davoine, G. Gallot, J.-P. Goddet, E. Lefebvre, V. Malka, and J. Faure, *Few Femtosecond, Few Kiloampere Electron Bunch Produced by a Laser Plasma Accelerator*, *Nat. Phys.* **7**, 219 (2011).
  - [10] A. Buck, M. Nicolai, K. Schmid, C. M. S. Sears, A. Sävert, J. M. Mikhailova, F. Krausz, M. C. Kaluza, and L. Veisz, *Real-Time Observation of Laser-Driven Electron Acceleration*, *Nat. Phys.* **7**, 543 (2011).
  - [11] J. P. Couperus, R. Pausch, A. Köhler, O. Zarini, J. M. Krämer, M. Garten, A. Huebl, R. Gebhardt, U. Helbig, S. Bock, K. Zeil, A. Debus, M. Bussmann, U. Schramm, and

- A. Irman, *Demonstration of a Beam Loaded Nanocoulomb-Class Laser Wakefield Accelerator*, *Nat. Commun.* **8**, 487 (2017).
- [12] J. Faure, C. Rechatin, A. Norlin, A. Lifschitz, Y. Glinec, and V. Malka, *Controlled Injection and Acceleration of Electrons in Plasma Wakefields by Colliding Laser Pulses*, *Nature (London)* **444**, 737 (2006).
- [13] K. Schmid, A. Buck, C. M. S. Sears, J. M. Mikhailova, R. Tautz, D. Herrmann, M. Geissler, F. Krausz, and L. Veisz, *Density-Transition Based Electron Injector for Laser Driven Wakefield Accelerators*, *Phys. Rev. ST Accel. Beams* **13**, 091301 (2010).
- [14] A. J. Gonsalves, K. Nakamura, C. Lin, D. Panasenko, S. Shiraishi, T. Sokollik, C. Benedetti, C. B. Schroeder, C. G. R. Geddes, J. van Tilborg, J. Osterhoff, E. Esarey, C. Tóth, and W. P. Leemans, *Tunable Laser Plasma Accelerator Based on Longitudinal Density Tailoring*, *Nat. Phys.* **7**, 862 (2011).
- [15] M. Fuchs, R. Weingartner, A. Popp, Z. Major, S. Becker, J. Osterhoff, I. Cortie, B. Zeitler, R. Hörlein, G. D. Tsakiris, U. Schramm, T. P. Rowlands-Rees, S. M. Hooker, D. Habs, F. Krausz, S. Karsch, and F. Grüner, *Laser-Driven Soft-X-Ray Undulator Source*, *Nat. Phys.* **5**, 826 (2009).
- [16] S. Kneip *et al.*, *Bright Spatially Coherent Synchrotron X-Rays from a Table-Top Source*, *Nat. Phys.* **6**, 980 (2010).
- [17] J. Wenz, S. Schleede, K. Khrennikov, M. Bech, P. Thibault, M. Heigoldt, F. Pfeiffer, and S. Karsch, *Quantitative X-Ray Phase-Contrast Microtomography from a compact laser-driven betatron source*, *Nat. Commun.* **6**, 7568 (2015).
- [18] K. Khrennikov, J. Wenz, A. Buck, J. Xu, M. Heigoldt, L. Veisz, and S. Karsch, *Tunable All-Optical Quasimonochromatic Thomson X-Ray Source in the Nonlinear Regime*, *Phys. Rev. Lett.* **114**, 195003 (2015).
- [19] C. B. Schroeder, E. Esarey, C. G. R. Geddes, C. Benedetti, and W. P. Leemans, *Physics Considerations for Laser-Plasma Linear Colliders*, *Phys. Rev. ST Accel. Beams* **13**, 101301 (2010).
- [20] M. E. Couprie, *New Generation of Light Sources: Present and Future*, *J. Electron Spectrosc. Relat. Phenom.* **196**, 3 (2014).
- [21] S. Corde, K. T. Phuoc, G. Lambert, R. Fitour, V. Malka, A. Rousse, A. Beck, and E. Lefebvre, *Femtosecond X Rays from Laser-Plasma Accelerators*, *Rev. Mod. Phys.* **85**, 1 (2013).
- [22] A. R. Maier, A. Meseck, S. Reiche, C. B. Schroeder, T. Seggebrock, and F. Grüner, *Demonstration Scheme for a Laser-Plasma-Driven Free-Electron Laser*, *Phys. Rev. X* **2**, 031019 (2012).
- [23] N. Delbos, C. Werle, I. Dornmair, T. Eichner, L. Hübner, S. Jalas, S. W. Jolly, M. Kirchen, V. Leroux, P. Messner, M. Schnepp, M. Trunk, P. A. Walker, P. Winkler, and A. R. Maier, *LUX—A laser-plasma driven undulator beamline*, *Nucl. Instrum. Methods Phys. Res., Sect. A* **909**, 318 (2018).
- [24] A. Pak, K. A. Marsh, S. F. Martins, W. Lu, W. B. Mori, and C. Joshi, *Injection and Trapping of Tunnel-Ionized Electrons into Laser-Produced Wakes*, *Phys. Rev. Lett.* **104**, 025003 (2010).
- [25] C. McGuffey, A. G. R. Thomas, W. Schumaker, T. Matsuoka, V. Chvykov, F. J. Dollar, G. Kalintchenko, V. Yanovsky, A. Maksimchuk, K. Krushelnick, V. Y. Bychenkov, I. V. Glazyrin, and A. V. Karpeev, *Ionization Induced Trapping in a Laser Wakefield Accelerator*, *Phys. Rev. Lett.* **104**, 025004 (2010).
- [26] M. Chen, E. Esarey, C. B. Schroeder, C. G. R. Geddes, and W. P. Leemans, *Theory of Ionization-Induced Trapping in Laser-Plasma Accelerators*, *Phys. Plasmas* **19**, 033101 (2012).
- [27] See Supplemental Material at <http://link.aps.org/supplemental/10.1103/PhysRevX.10.031039> for details on the electron spectrum post processing.
- [28] W. Lu, M. Tzoufras, C. Joshi, F. S. Tsung, W. B. Mori, J. Vieira, R. A. Fonseca, and L. O. Silva, *Generating Multi-GeV Electron Bunches Using Single Stage Laser Wakefield Acceleration in a 3D Nonlinear Regime*, *Phys. Rev. ST Accel. Beams* **10**, 061301 (2007).
- [29] D. A. Alessi, P. A. Rosso, H. T. Nguyen, M. D. Aasen, J. A. Britten, and C. Haefner, *Active Cooling of Pulse Compression Diffraction Gratings for High Energy, High Average Power Ultrafast Lasers*, *Opt. Express* **24**, 30015 (2016).
- [30] V. Leroux, S. W. Jolly, M. Schnepp, T. Eichner, S. Jalas, M. Kirchen, P. Messner, C. Werle, P. Winkler, and A. R. Maier, *Wavefront Degradation of a 200 TW Laser from Heat-Induced Deformation of in-Vacuum Compressor Gratings*, *Opt. Express* **26**, 13061 (2018).
- [31] V. Leroux, T. Eichner, and A. R. Maier, *Description of Spatio-temporal Couplings from Heat-Induced Compressor Grating Deformation*, *Opt. Express* **28**, 8257 (2020).